Reduction of endoplasmic reticulum stress attenuates the defects caused by *Drosophila* mitofusin depletion

Valentina Debattisti,[1] Diana Pendin,[2] Elena Ziviani,[3] Andrea Daga,[2] and Luca Scorrano[1,4]

[1]Dulbecco Telethon Institute, Venetian Institute of Molecular Medicine, 35129 Padua, Italy
[2]Eugenio Medea Scientific Institute, 31015 Conegliano, Italy
[3]Department of Cell Physiology and Metabolism, University of Geneva, 1205 Geneva, Switzerland
[4]Department of Biology, University of Padua, 35121 Padua, Italy

Ablation of the mitochondrial fusion and endoplasmic reticulum (ER)–tethering protein Mfn2 causes ER stress, but whether this is just an epiphenomenon of mitochondrial dysfunction or a contributor to the phenotypes in mitofusin (Mfn)-depleted *Drosophila melanogaster* is unclear. In this paper, we show that reduction of ER dysfunction ameliorates the functional and developmental defects of flies lacking the single Mfn mitochondrial assembly regulatory factor (Marf). Ubiquitous or neuron- and muscle-specific Marf ablation was lethal, altering mitochondrial and ER morphology and triggering ER stress that was conversely absent in flies lacking the fusion protein optic atrophy 1. Expression of Mfn2 and ER stress reduction in flies lacking Marf corrected ER shape, attenuating the developmental and motor defects. Thus, ER stress is a targetable pathogenetic component of the phenotypes caused by *Drosophila* Mfn ablation.

Introduction

In mammalian cells, mitochondria and ER are juxtaposed, generating an interface crucial for mitochondrial Ca^{2+} uptake, lipid transfer between the two organelles, mitochondrial fission, and autophagosome formation (de Brito and Scorrano, 2008; Friedman et al., 2011; Area-Gomez et al., 2012; Hamasaki et al., 2013). This juxtaposition is mediated in yeast by a multiprotein complex called ER–mitochondria encounter structure (Kornmann et al., 2009) and in mammals by Mfn2 (de Brito and Scorrano, 2008) and other indirect bridges (de Brito and Scorrano, 2010). Mfn2, like its homologous Mfn1, is a large outer membrane GTPase that fuses mitochondria (Santel and Fuller, 2001; Santel et al., 2003) in cooperation with the inner membrane protein optic atrophy 1 (Opa1; Olichon et al., 2002; Cipolat et al., 2004). Functionally, *Mfn2* ablation reduces ER–mitochondria tethering, mitochondrial Ca^{2+} uptake, and lipid transfer (de Brito and Scorrano, 2008; Area-Gomez et al., 2012) and causes ER stress (Sebastián et al., 2012), highlighting the importance of the juxtaposition for the function of both organelles. However, because ER stress can be caused by mitochondrial dysfunction (Ishikawa et al., 2009), the *Mfn2$^{-/-}$* ER perturbations could be mere epiphenomena of the *Mfn2$^{-/-}$* mitochondrial defects, and as such, their contribution to the phenotypes caused by *Mfn2* loss might be marginal.

Drosophila melanogaster seems a suitable model to address this question. In addition to *Fzo* (*fuzzy onions*), the spermatocyte-specific mitofusin (Mfn) responsible for the formation of the giant flagellum mitochondria (Hales and Fuller, 1997), it possesses a ubiquitous Mfn-christened *Mitochondrial assembly regulatory factor* (*Marf*; Hwa et al., 2002; Deng et al., 2008; Ziviani et al., 2010). *Marf* ablation is lethal at the larval stage, and its selective down-regulation in the heart disrupts mitochondrial morphology and cardiac function (Dorn et al., 2011). We therefore asked whether and to which extent ER function contributes to the Marf ablation phenotypes. Our data support a crucial role for ER stress, suggesting that it might be a therapeutic target in CMTIIa (Charcot–Marie–Tooth type 2a) disease in which Mfn is malfunctioning.

The Rockefeller University Press $30.00
J. Cell Biol. Vol. 204 No. 3   303–312
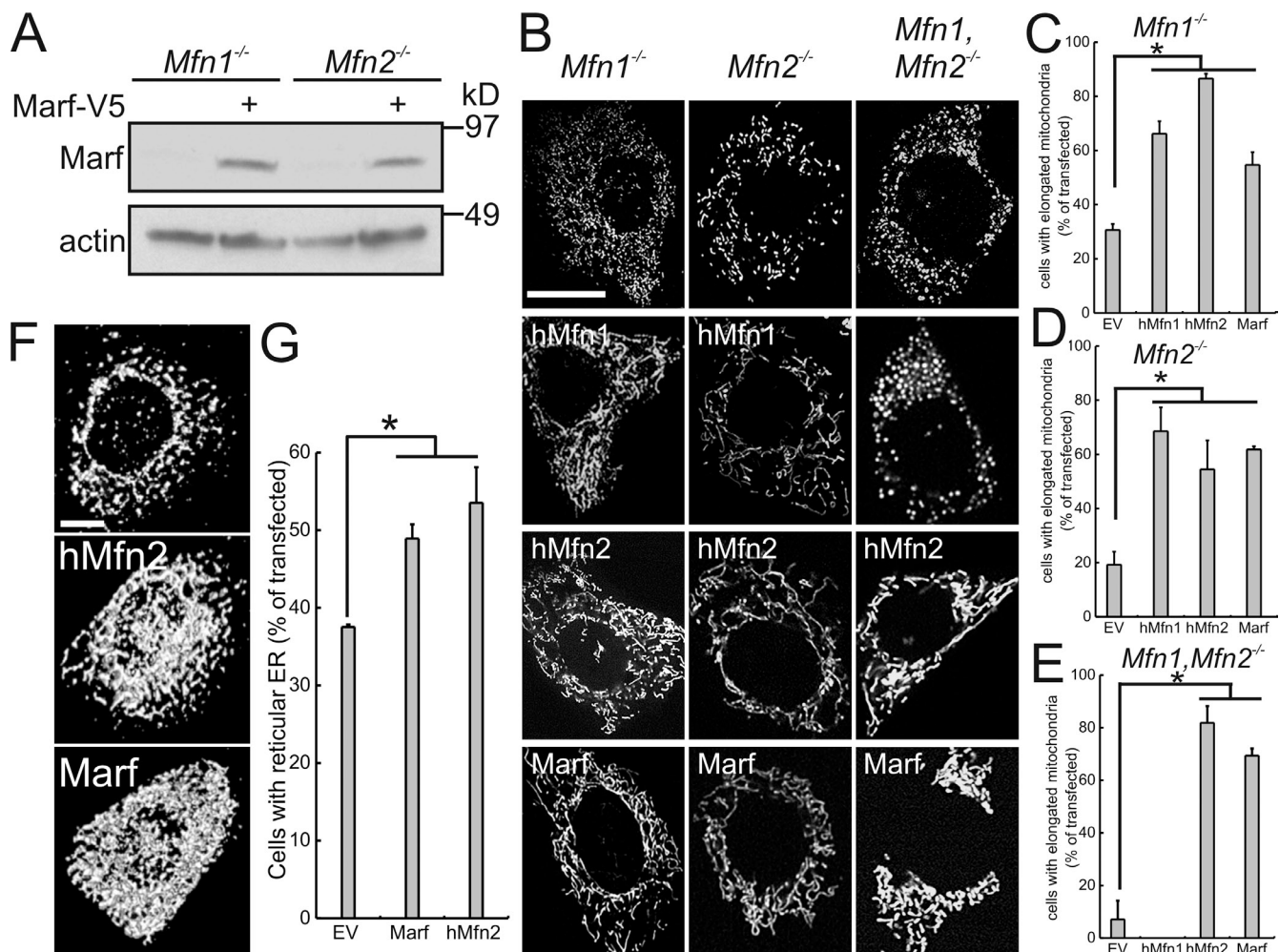www.jcb.org/cgi/doi/10.1083/jcb.201306121

JCB   303

Figure 1. **_Drosophila_ Marf complements Mfn-deficient mouse cells.** (A) Equal amounts of proteins (50 µg) from MEFs of the indicated genotype transfected as indicated were separated by SDS-PAGE and immunoblotted using the indicated antibodies. (B) Representative confocal images of MEFs of the indicated genotype cotransfected with mtYFP and the indicated plasmid. (C–E) Means ± SEM of four independent experiments of mitochondrial morphometry as in B. *, P < 0.05, two-tailed Student's _t_ test versus empty vector (EV). (F) Representative 3D reconstructions of ER in _Mfn2_$^{-/-}$ MEFs cotransfected with ER-YFP and the indicated plasmid. (G) Means ± SEM of four independent experiments as in F. *, P < 0.05, two-tailed Student's _t_ test versus empty vector. Bars, 15 µm.

Results and discussion

To explore the relative role of ER and mitochondria in the Mfn ablation phenotype, _Drosophila_ would be a suitable model only if the ER-modulating function of Mfns did not emerge in evolution later than Marf. We therefore set out to address whether Marf can shape both mitochondria and ER. Expression of comparable Marf levels (Fig. 1 A) in mouse embryonic fibroblasts (MEFs) lacking _Mfn1_ and/or _Mfn2_ (Chen et al., 2003) restored the elongated mitochondrial morphology as efficiently as human Mfns (hMfns; Fig. 1, B–E). The altered _Mfn2_$^{-/-}$ ER morphology is selectively recovered by hMfn2, independently of its ability to correct mitochondrial shape (de Brito and Scorrano, 2008). By inspecting 3D-reconstructed, volume-rendered images from confocal stacks of ER-targeted YFP (ER-YFP), we noted that Marf-V5 recovered _Mfn2_$^{-/-}$ ER morphology as efficiently as hMfn2 (Fig. 1, F and G). Accordingly, effective _Marf_ knockdown in _Drosophila_ S2R+ cells (Fig. S1 A) caused mitochondrial fragmentation (Fig. S1 B) and ER fragmentation

and clumping (Fig. S1 C), which were complemented by the reexpression of an RNAi-resistant mutant of Marf (Fig. S1, F and E), substantiating that the phenotypes observed are specifically caused by Marf loss. Thus, _Drosophila_ Mfn modulates both mitochondrial and ER morphology.

We next moved our analysis of mitochondrial and ER shape to in vivo, taking advantage of upstream activation sequence (UAS)-_Marf_[RNAi] transgenic flies, in which we could control expression of _Marf_ RNAi in space and time using the Gal4-UAS system (Brand and Perrinon, 1993). Because our RNAi was specific (Fig. S1) and efficiently ablated _Marf_ in vivo (Fig. 2 A), we explored whether Marf loss altered development. Ubiquitous, tubulin-Gal4–driven Marf down-regulation was lethal, arresting development at the second instar larvae stage (unpublished data). Taking advantage of crosses between the UAS-_Marf_[RNAi] flies and lines carrying both a UAS–mitochondrial GFP (mtGFP) and the Gal4 transgene under the control of different tissue-specific promoters, we noticed that in ubiquitous _Marf_[RNAi] larvae, mitochondria were clustered and fragmented
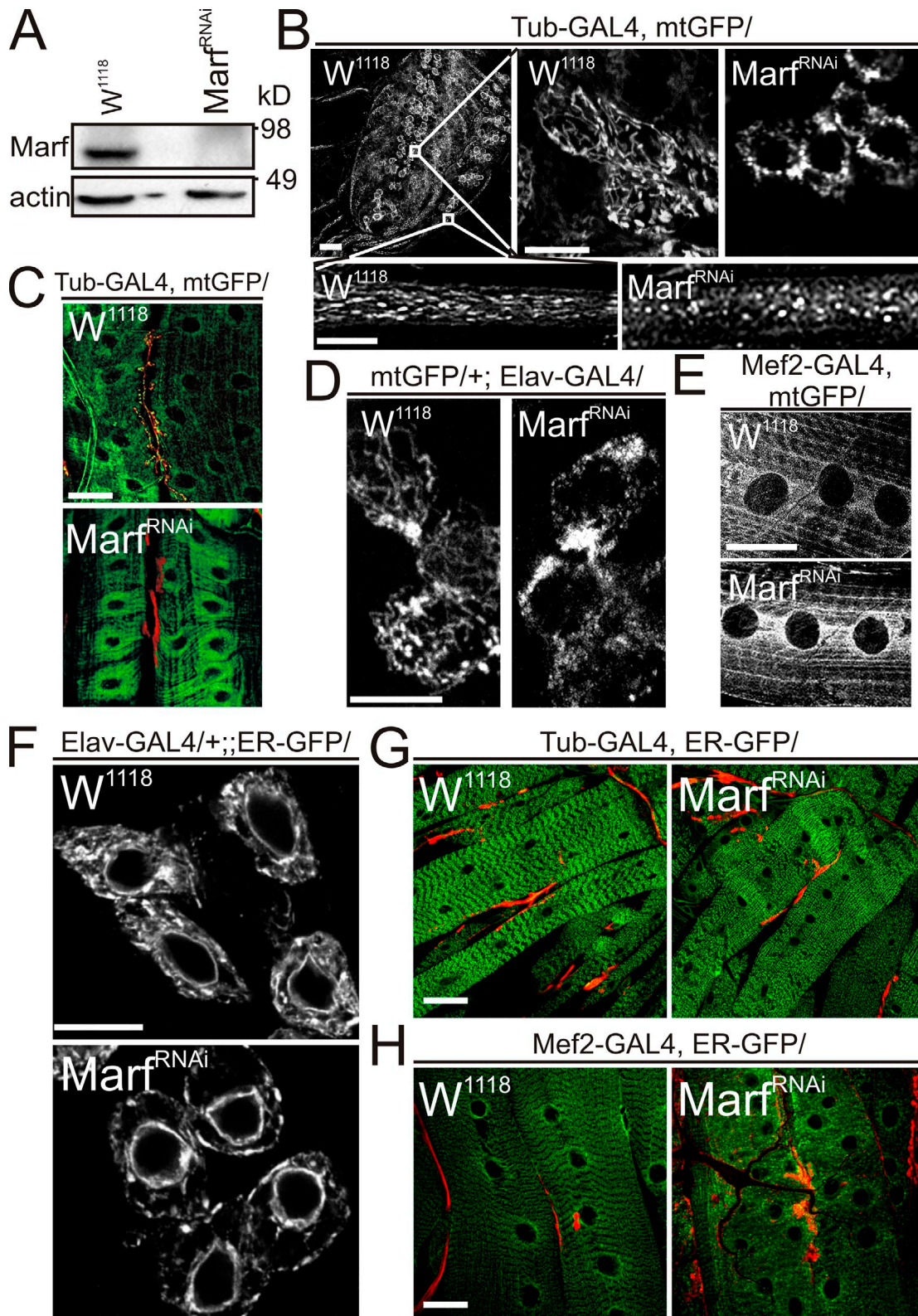
Figure 2. **Ubiquitous, neuronal, or muscular Marf ablation alters mitochondrial and ER morphology.** (A) Equal amounts of protein (50 µg) from tubulin (Tub)-Gal4/+ (W[1118]) and tubulin-Gal4/UAS-Marf[RNAi] (Marf[RNAi]) larvae separated by SDS-PAGE were immunoblotted using the indicated antibodies. (B) Representative ventral ganglion mtGFP confocal images from the indicated larvae. Higher magnifications of the boxed neuronal cell bodies (right) and axons located in the proximity of the ventral ganglion (bottom) are shown. (C) Maximum projections of stacks of confocal mtGFP images from muscles 6 and 7 of the indicated larvae (neuromuscular junctions [NMJs] labeled with HRP, red). (D and E) Representative mtGFP confocal images in neuronal cell bodies (D) and body wall muscles (E) of the indicated larvae. (F) Representative ER-GFP confocal images in neuronal cell bodies of the indicated larvae. (G and H) Representative confocal ER-GFP images from muscles 6 and 7 (NMJs labeled with HRP, red) of the indicated larvae. Bars: (B–D and F) 10 µm; (E, G, and H) 20 µm.
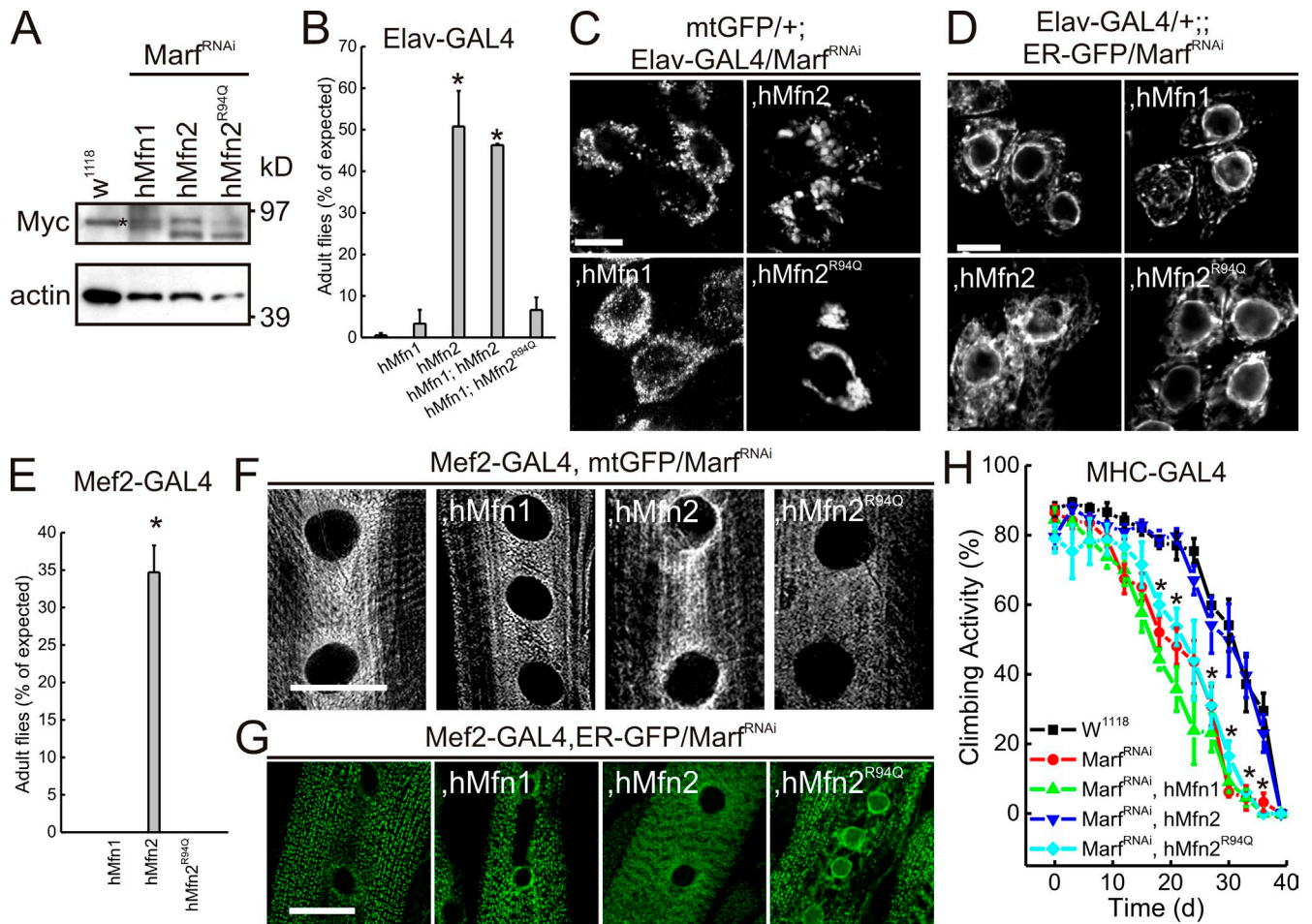
Figure 3. **hMfn2 complements *Drosophila* Marf.** (A) Equal amounts of protein (50 µg) from larval brains of Elav-Gal4/+ (W[1118]), Elav-Gal4/UAS-Marf[RNAi], UAS-hMfn2 (hMfn2), Elav-Gal4/UAS-Marf[RNAi], UAS-hMfn2[R94Q] (hMfn2[R94Q]), and Elav-Gal4/UAS-Marf[RNAi], UAS-hMfn1 (hMfn1) were separated by SDS-PAGE and immunoblotted using the indicated antibodies. The asterisk indicates an unspecific band. (B) Viability of Elav-Gal4/TM6 flies mated to UAS-Marf[RNAi] lines carrying the indicated *UAS* insertion measured as the TM6^{−}/TM6^{+} ratio (*n* > 100 for each genotype). Data represent means ± SEM of three independent matings. *, P < 0.05 in a two-tailed Student's *t* test with UAS-Marf[RNAi]/Elav-Gal4 (−). (C) Maximum projections of confocal stacks of mtGFP from neuronal cell bodies of the indicated larvae. (D) ER-GFP confocal images from neuronal cell bodies of the indicated larvae. (E) Viability of Mef2-Gal4/TM6 flies mated to UAS-Marf[RNAi] lines carrying the indicated *UAS* insertion measured as the TM6^{−}/TM6^{+} ratio (*n* > 100 for each genotype). Data represent means ± SEM of three independent matings. *, P < 0.05 in a Student's *t* test against UAS-Marf[RNAi]/Mef2-Gal4 (−). (F) Representative mtGFP confocal images in body wall muscles of the indicated larvae. (G) Confocal ER-GFP images in muscles 6 and 7 in which NMJs have been labeled with α-HRP (red) of larvae of the indicated genotype. (H) Climbing performance of MHC-Gal4 homozygous flies mated to the indicated homozygous lines. For each genotype, ≥50 flies were assessed for the assay. Data are means ± SEM of five independent experiments. *, P < 0.05 in a Student's *t* test against MHC-Gal4/+ (W[1118]) and against MHC-Gal4/+;; UAS-hMfn2, UAS-Marf[RNAi]/+ (hMfn2). Bars: (C, D, and F) 10 µm; (G) 20 µm.

in ventral ganglion neuronal cell bodies and small and clumped in ventral ganglion axons (Fig. 2 B). Likewise, in the smaller *Marf*[RNAi] muscles, mitochondria appeared clustered in the perinuclear region (Fig. 2 B). When we spatially restricted *Marf*[RNAi] expression using the neuronal Elav-Gal4 and the muscular Mef2-Gal4 driver lines (Ranganayakulu et al., 1996; Osterwalder et al., 2001), we observed different degrees of lethality but very similar mitochondrial morphological alterations. In the nervous system and in the muscle, *Marf* ablation was lethal at the pupa stage; however, some escapers (∼10%) reached adulthood when it was ablated in the muscle (unpublished data). Mitochondria were fragmented and clustered in neuronal cell bodies (Fig. 2 D) and lost their sarcomeric organization to clump around the nuclei (Fig. 2 E) in the muscle. Thus, Marf is essential for normal mitochondrial morphology in all the tissues in which we ablated it. To explore also whether ER shape was altered by Marf ablation

in vivo, we generated *Marf*[RNAi] lines carrying an ER fluorescent reporter (ER-GFP). In control ventral ganglion neuronal cell bodies, the ER appeared to be interconnected throughout the whole cytoplasm, and in the muscle, the sarcoplasmic reticulum (SR) displayed a typical sarcomeric organization with interconnected cisternae. Upon neuron-specific Marf ablation, fragmented ER cisternae accumulated in the cell cortex (Fig. 2 F). In muscles from ubiquitous (Fig. 2 G) and muscle-specific (Fig. 2 H) *Marf*[RNAi] larvae, the sarcomeric SR pattern was lost with punctiform and individual cisternae. The ER derangement was further supported by electron micrographs of Marf-ablated neuronal cell bodies showing dilated, fragmented ER cisternae (Fig. S3 A) and by assays of fluorescence loss in photobleaching (FLIP) in which ER-GFP diffusion was slower in *Marf*[RNAi] SR (Fig. S3, B and C), indicative of a loss of SR cisternae continuity. Our in vivo morphological analysis demonstrates that

Marf ablation affects mitochondrial as well as ER shape. The role of lower, nonmetazoan Mfns in ER shape is not explored, but it appears that Fzo1p, the *Saccharomyces cerevisiae* Mfn is not involved in ER–mitochondria tethering, performed instead by a specialized complex (Kornmann et al., 2009). Perhaps, in chordates, the requirement to separate ER–mitochondria tethering and cross talk from mitochondrial fusion in tissues pressured for the emergence of two Mfns: for example, in the heart, both Mfns are abundantly expressed (Santel et al., 2003), but although mitochondrial fusion is not apparent (Papanicolaou et al., 2011), Mfn2-dependent SR–mitochondrial juxtaposition is crucial for mitochondrial Ca^{2+} uptake (Chen et al., 2012), consistent with the impact of Mfn2 ablation on cardiomyocyte development (Kasahara et al., 2013). Our data show that the primordial metazoan Mfn regulates mitochondrial as well as ER shape (and ER–mitochondria tethering in S2 cells; unpublished data), indicating in Marf the potential ancestor of the two functionally different chordate Mfns.

We wished to dissect the relative contribution of the co-existing mitochondrial and ER alterations to the phenotypes of *Marf*[RNAi] flies. We started by verifying whether hMfn 1 and 2, which differ in their ability to modulate ER morphology and cross talk with mitochondria (de Brito and Scorrano, 2008; Cerqua et al., 2010; De Stefani et al., 2011; Chen et al., 2012; Ngoh et al., 2012), were equally efficient in complementing *Marf*[RNAi] flies. We generated UAS transgenic lines for the ectopic expression of Myc-tagged hMfn1, hMfn2, or hMfn2[R94Q], a mutation associated with CMTIIA neuropathy (Züchner et al., 2004; Detmer et al., 2008; Cartoni et al., 2010) that complements *Mfn2*^{−/−} mitochondrial, but not ER, defects (Detmer and Chan, 2007; de Brito and Scorrano, 2008). Because neuronal- and muscle-specific hMfn expression was compatible with life (unpublished data), we drove neuronal or muscle expression of UAS-*Marf*[RNAi] and UAS-hMfns-Myc. Although the three hMfns were expressed at comparable levels in the transgenic larvae brain (Fig. 3 A), only hMfn2 partially rescued the *Marf*[RNAi] lethality, allowing survival to adulthood of ~50% of the individuals. hMfn2 efficacy was not increased by coexpression with hMfn1, which alone or with hMfn2[R94Q]—a combination that fully complements *Mfn2*^{−/−} mitochondrial, but not ER, morphology (Detmer and Chan, 2007; de Brito and Scorrano, 2008)—was unable to rescue *Marf*[RNAi] lethality (Fig. 3 B). In hMfn2-expressing *Marf*[RNAi] flies, neuronal cell body mitochondria were fragmented, but ER morphology was restored (Fig. 3, C and D; and Fig. S3 C, electron microscopy). The picture was similar in muscle-specific *Marf*[RNAi] flies: only hMfn2 could partially rescue the developmental defect (Fig. 3 D) and restored SR, but not mitochondrial, morphology (Fig. 3, E and F).

We wished to extend these data by addressing whether hMfn2 could also functionally rescue *Marf*[RNAi] flies. Using the weak myosin heavy chain (MHC)–Gal4 promoter, we could obtain muscle-specific *Marf*[RNAi] adult individuals. In these muscle-specific *Marf*[RNAi] flies, hMfn2 selectively corrected the SR dysmorphology (Fig. S3 D) and, in a routinely used test for *Drosophila* locomotor performance (Orso et al., 2009), rescued the impaired climbing performance of *Marf*[RNAi] flies (Fig. 3 G). Thus, hMfn2 complements *Marf*[RNAi] fly development and function, correcting

their ER shape. Our model of weak muscle Mfn ablation appears useful to screen for genetic interactors that ameliorate the climbing performance, impossible in the available mouse models of CMTIIa (Detmer et al., 2008; Cartoni et al., 2010), and to screen for drugs that might ameliorate the locomotor phenotype.

Having established that ER shape defects correlate with *Marf*[RNAi] fly climbing defects, we wondered whether ER dysmorphology was accompanied by ER stress. The prototypical ER stress inducer DTT switched on a genetically encoded GFP reporter of the ER stress transcription factor Xbp1 (Ryoo et al., 2007, 2013) in numerous neurons of treated larvae. Likewise, GFP-positive neurons were found when this reporter line was crossed with the *Marf*[RNAi] flies (Fig. 4 A). Another marker, the ER stress-induced chaperone binding Ig protein (BiP), accumulated in muscles and neurons upon ubiquitous *Marf* ablation (Fig. 4 B). ER stress was not, however, a common response to mitochondrial fusion ablation because, in flies lacking *Opa1*, the GFP Xbp1 reporter was not activated (Fig. 4 A), and the levels of BiP were normal (Fig. 4 B). To assess the contribution of ER stress to the *Marf*[RNAi] phenotype, we turned to flies expressing a constitutively spliced Xbp1 variant (mXbp1s) that ameliorates phenotypes caused by ER stress in flies (Casas-Tinto et al., 2011). Expression of mXbp1s partially rescued the developmental defect of *Marf*[RNAi] flies (Fig. 4 C), ameliorating ER and SR, but not mitochondrial, morphology in ubiquitous (Fig. 4, D and E) and muscle-specific *Marf*[RNAi] individuals (Fig. 4, F and G). Most importantly, once expressed in muscle-specific *Marf*[RNAi] flies, Xbp1s corrected the impaired climbing performance (Fig. 4 H). The conclusions from these genetic experiments were further corroborated when we observed that the chemical chaperones tauroursodeoxycholic acid (TUDCA) and 4-phenylbutyric acid (PBA), which reduce ER stress in vitro and in vivo (Ozcan et al., 2006; Solá et al., 2003; Inden et al., 2007; Sebastián et al., 2012), reduced ER stress, ameliorated development, and improved climbing of *Marf*[RNAi] flies (Fig. 5). Collectively, our data indicate that genetic and pharmacological ER stress manipulation is sufficient to restore ER morphology and locomotor function in *Marf*[RNAi] *Drosophila*.

In principle, the ER stress and fragmentation observed in Marf-deficient tissues could be secondary to mitochondrial dysfunction as, for example, it was reported for a mouse model of myopathy (Irwin et al., 2003). However, multiple evidence support a specific role for Marf in ER function: (a) *Opa1* ablation does not cause ER stress; (b) hMfn2 selectively complements ER, but not mitochondrial, shape in *Marf*[RNAi] flies; and (c) Marf ablation resembles the ER stress caused by *Mfn2* ablation in mammals (Ngoh et al., 2012), with far-reaching implications for insulin production (Sebastián et al., 2012) and neuronal control of metabolism (Schneeberger et al., 2013).

Our analysis substantiates a model in which Mfn2 regulates ER shape and function also in the fruit fly. Despite the numerous functional differences between Mfn1 and Mfn2 (Ishihara et al., 2004; de Brito and Scorrano, 2008; Tondera et al., 2009; Cerqua et al., 2010; De Stefani et al., 2011; Chen et al., 2012; Ngoh et al., 2012), they are believed to be functionally interchangeable (Detmer and Chan, 2007). Our data show in vivo that the two Mfns are functionally different and indicate that ER

Figure 4. ER stress participates in *Marf*^{RNAi} developmental and functional impairment. (A) Maximum projections of confocal z stacks of the ventral ganglion of larvae of the indicated genotype crossed with the ER stress reporter line UAS-Xbp1-EGFP (green). When indicated, larvae were treated for 4 h with 500 µM DTT. Red, α-Hrp staining. Act, Actin; Tub, tubulin. (B) Representative confocal images of ventral ganglion (top) and body wall muscles (bottom) of larvae of the indicated genotype stained with α-BiP. (C) Development of tubulin-Gal4/TM6 flies (left, ;;Marf^{RNAi}/+) and Mef2/TM6 (right, ;;Opa1^{RNAi}/+) crossed to homozygous individuals of the indicated genotype measured as the TM6⁻/TM6⁺ ratio (n > 70 for each genotype). Data represent means ± SEM of four independent matings. *, P < 0.05 in a two-tailed Student's *t* test with +/+; tubulin-Gal4/UAS-Marf^{RNAi} (+/+). (D) Maximum projections of mtGFP confocal stacks in neuronal cell bodies (top) and in NMJs from muscles 6 and 7 labeled with HRP (blue; bottom) in the indicated larvae. (E) Confocal ER-GFP images in neuronal cell bodies (top) and in muscles 6 and 7 (bottom) of the indicated larvae. (F) Confocal images of ATP synthase, subunit α in body wall muscles of the indicated larvae. (G) Confocal images of atlastin in body wall muscles of the indicated larvae genotype. (H) Climbing performance of MHC-Gal4 homozygous flies mated to the indicated homozygous lines. Data are means ± SEM of five independent experiments (n > 50 flies per genotype per experiment). *, P < 0.05 in a Student's *t* test against W¹¹¹⁸ and mXbp1s;Marf^{RNAi}. Bars: (A, B, D, F, and G) 10 µm; (E) 20 µm.
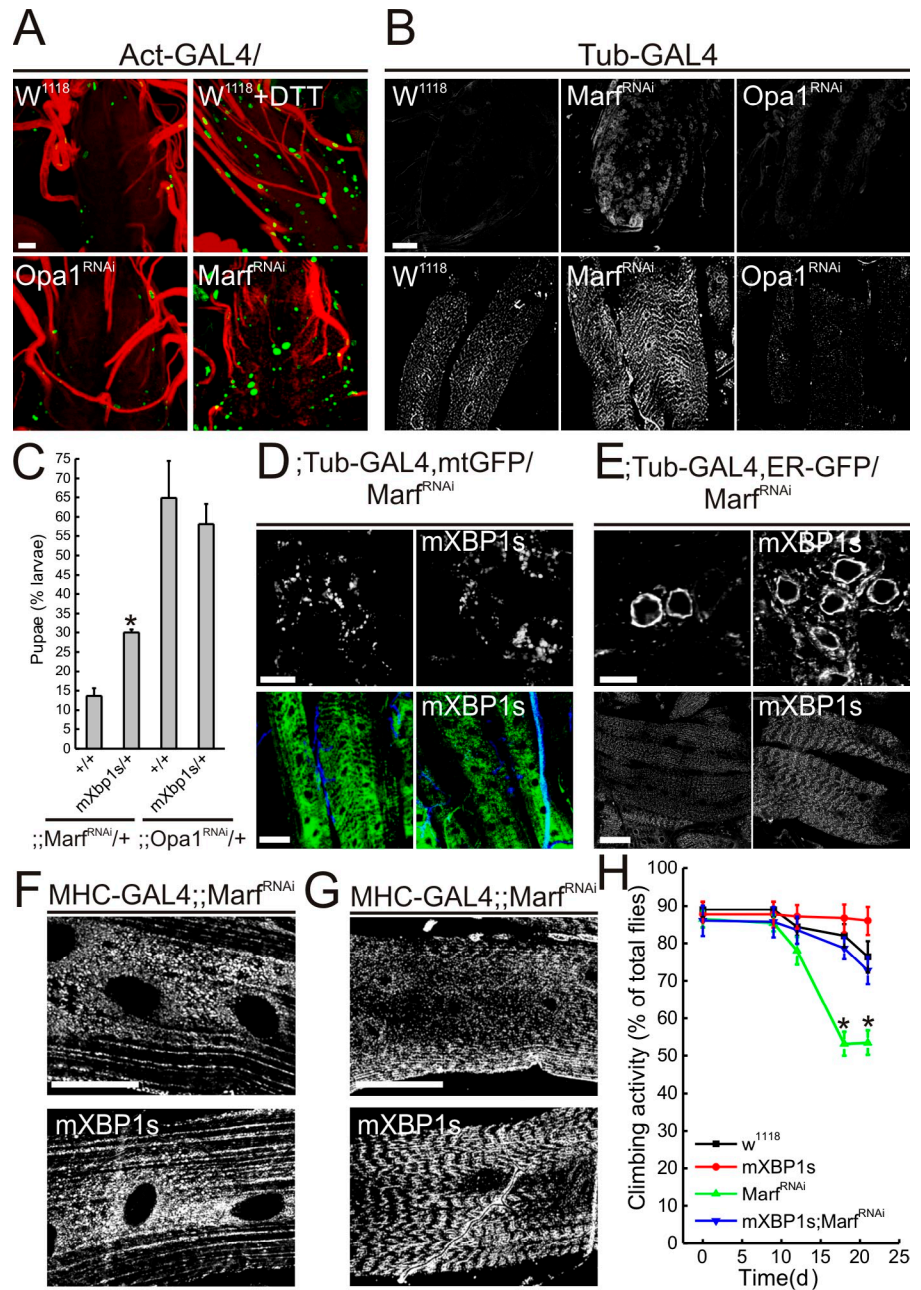
shape and function are regulated only by Mfn2. Our genetic analysis indicates that the metazoan Marf harbors both mitochondria- and ER-shaping functions of mammalian Mfns.

ER stress attenuation emerges as a new potential pharmacological target for CMTIIa in which Mfn2 is mutated and for other conditions in which it is malfunctioning. In a proof-of-principle experiment, the locomotor defects of flies lacking Marf in the muscle were corrected by two ER chemical chaperones, including TUDCA, an already FDA-approved drug that holds potential to be further tested in CMTIIa models.

Materials and methods

Drosophila genetics and strains
To obtain transgenic lines, Myc-Mfn1, Myc-Mfn2, and Myc-hMfn2^{R94Q} cDNAs from the pcB6 vector were subcloned in the pUAST transformation vector, and several transgenic lines for each construct were generated by microinjection of *Drosophila* embryos (BestGene, Inc.). Transgenic lines were then characterized and balanced to obtain a stable transgenic line. The *Drosophila* strains used were Elav-Gal4, tubulin-Gal4 (Bloomington Stock Center), UAS-Marf^{RNAi} (transformant ID 40478 [Marf^{RNAi}] and transformant ID 105261 [Marf^{RNAi-II}]; Vienna Drosophila RNAi Center), Mef2-Gal4, MHC-Gal4, Actin-Gal4, pUASp:Lys-GFP-KDEL (UAS–ER-GFP; a gift from J. Lippincott-Schwartz, National Institute of Child Health and Human Development, National Institutes of Health, Bethesda, MA; Snapp et al., 2004), UAS-mtGFP (a gift from W. Saxton, University of California, Santa Cruz, Santa Cruz, CA), UAS-Xbp1-EGFP (a gift from H. Steller, The Rockefeller University, New York, NY; Ryoo et al., 2007), and UAS-mXbp1s (a gift from D. Rincon-Limas, University of Florida College of Medicine, Gainesville, FL; Casas-Tinto et al., 2011). Control genotypes varied depending on individual experiments but always included promoter Gal4/+ and UAS transgene/+ individuals.

Molecular biology
mtYFP (pEYFP-mitochondria [mito]) and ER-YFP (pEYFP-ER) were purchased from Takara Bio, Inc. Mitochondrial targeted DsRED (mtRFP) was a gift from T. Pozzan (Venetian Institute of Molecular Medicine, Padua, Italy; Cipolat
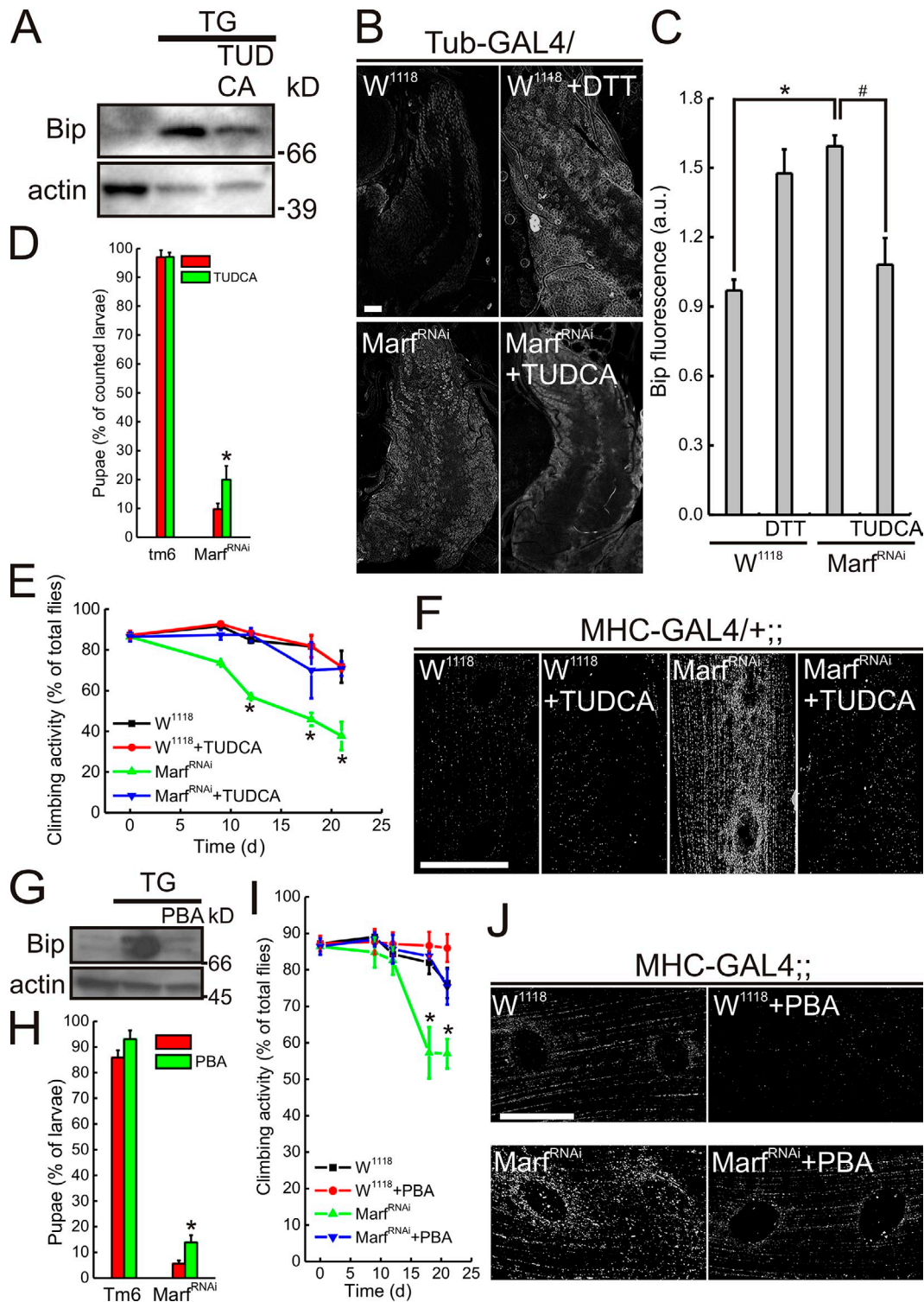
Figure 5. **The chemical ER chaperones TUDCA and PBA correct ER stress and climbing defect of Marf[RNAi] flies.** (A) Equal amounts of protein (50 μg) from S2R+ cells treated as indicated were separated by SDS-PAGE and immunoblotted with the indicated antibodies. TG, thapsigargin. (B) Confocal BiP images of ventral ganglion of larvae treated as indicated. Tub, tubulin. (C) Quantification of α-BiP fluorescence in experiments as in B. Data are means ± SEM of three independent experiments. *, P < 0.05 in a two-tailed Student's t test; #, P < 0.05 in a paired Student's t test. a.u., arbitrary unit. (D) Percentage of larvae reaching pupa stage from tubulin-Gal4/TM6 flies crossed to homozygous UAS-Marf[RNAi] (Marf[RNAi]) individuals fed as indicated ($n > 70$ for each genotype). Data are means ± SEM of seven independent experiments. *, P < 0.05 in a paired Student's t test against Marf[RNAi]. (E) Climbing performance of MHC-Gal4 homozygous flies mated to W[1118] or to UAS-Marf[RNAi] (Marf[RNAi]) homozygous individuals fed as indicated. Data are means ± SEM of three independent experiments. *, P < 0.05 in a two-tailed Student's t test against W[1118] and in a paired Student's t test against Marf[RNAi] + TUDCA (F) Confocal BiP images of body wall muscles of MHC-Gal4/+ (W[1118]) and MHC-Gal4/+;;UAS-Marf[RNAi]/+ (Marf[RNAi]) larvae fed as indicated. (G) Immunoblots were as in A. (H) Experiments were as in D. Data are means ± SEM of seven independent experiments. *, P < 0.05 in a paired Student's t test against Marf[RNAi]. (I) Experiments were as in E. *, P < 0.05 in a two-tailed Student's t test against W[1118] and in a paired Student's t test against Marf[RNAi] + PBA. (J) Experiments were as in F. Where indicated, individuals were fed with PBA. Bars, 10 μm.

et al., 2004). pcB6-Myc-Mfn1 and pcB6-Myc-Mfn2 were a gift from M. Rojo (Salpetriere Hospital, Paris, France; de Brito and Scorrano, 2008).

Total RNA from adult *Drosophila* heads was purified with TRIZOL (Invitrogen). The *Marf* full-length cDNA was obtained by RT-PCR performed on total *Drosophila* head RNA. The full-length cDNA of Marf was first cloned in pDONR221 (Invitrogen) and then into pcDNA3.2/V5-DEST by Gateway cloning (Invitrogen). pAc5.1-Atl^TM-GFP was generated by cloning the 120 amino acids of the transmembrane domain of *Drosophila* atlastin (Orso et al., 2009) into pAc5.1/V5-His (Invitrogen), previously modified with the insertion of the EGFP sequence from the pEGFP-N1 vector (Takara Bio Inc.). mtGFP was generated by subcloning the cDNA from pEGFP-mito (Takara Bio Inc.) into pActin-PPA. For generation of double-stranded RNA (dsRNA)–resistant mutant of Marf (Marf-RNAi^R). Invariant-coding mutagenesis A → T84 and A → T90 of pAc5.1/V5-His-Marf was performed by using the site-directed mutagenesis kit (QuikChange; Agilent Technologies).

Generation of the anti-Marf antibody

pGEX expression vector was used to produce a synthetic peptide corresponding to the first 367 amino acid residues of the Marf protein sequence. The immunization of rabbits for antibody production was performed by Davids Biotechnologie. Specificity of antisera was tested on S2R cell extracts.

Cell culture

Mfn1^−/− and *Mfn2*^−/− MEFs were obtained from D. Chan (California Institute of Technology, Pasadena, CA) and cultured as previously described (Chen et al., 2003, 2005). Transfection was performed using a lipid reagent (TransFectin; Bio-Rad Laboratories) according to the manufacturer's instructions. S2R+ cells were cultured in Schneider's medium (Invitrogen) supplemented with 5% FBS (Sigma-Aldrich) and 1% penicillin–streptomycin (Invitrogen-Gibco). Transfection was performed using a reagent (FlyFectin; OZ Biosciences) according to the manufacturer's instructions.

RNAi

dsRNAs were prepared using the transcription kit (MEGAscript T7; Ambion). Primers used to generate two dsRNAs targeted to *Marf* were 5′-TTAATA-CGACTCACTATAGGGAGACCGAGGGCTTTCAGATACGCTACTTC-3′ and 5′-TTAATACGACTCACTATAGGGAGATTGACACCTTCTCCTCCACCT-CCTC-3′; and 5′-TTAATACGACTCACTATAGGGAGATGAGCAAATACC-CCCAAAAG-3′ and 5′-TTAATACGACTCACTATAGGGAGAGATCTGG-AGCGGTGATTTGT-3′. 1.2 × 10^6 S2R+ cells were treated daily with 10 μg of each dsRNA probe in serum-free medium and, after 2 h, transferred to complete medium.

Immunohistochemistry

Wandering third instar larvae raised at 25°C were harvested, dissected dorsally in standard saline, fixed in 4% paraformaldehyde or 4% formaldehyde for 10 min, and then washed in PBS containing 0.2 or 0.5% Triton X-100 and incubated with primary anti-HRP (1:500; Molecular Probes) or anti-BiP (1:50; Babraham Bioscience Technologies) antibody overnight at 4°C, whereas secondary antibodies (Cy3 anti–rat; 1:500; Jackson Immuno-Research Laboratories, Inc.) were incubated for 2 h at RT.

Imaging

Imaging experiments were always performed at 25°C. For confocal imaging, cells seeded onto 24-mm round glass coverslips, incubated in HBSS supplemented with 10 mM Hepes, were placed on the stage of an inverted microscope (Eclipse TE300; Nikon) equipped with a spinning-disk live-cell imaging confocal system (UltraVIEW; PerkinElmer), a piezoelectric z-axis motorized stage (PIFOC; Physik Instrumente), and a 12-bit charge-coupled device camera (Orca ER; Hamamatsu Photonics). Cells expressing ER-YFP or mtYFP were excited using the 488- or the 543-nm line of the HeNe laser (Modular Laser System; PerkinElmer) with exposure times of 50 ms by using a 60×, 1.4 NA Plan Apochromat objective (Nikon). For confocal z-axis stacks, stacks of 50 images separated by 0.2 μm along the z axis were acquired. Total acquisition time for each stack was 1.1 s to minimize reconstruction artifacts caused by movement of the ER. Images were then deconvolved using the convolve function of ImageJ (National Institutes of Health) and a custom 9 × 9 matrix. 3D reconstruction and volume rendering of the stacks were performed with the VolumeJ plugin of ImageJ by using the nearest neighbor interpolation function. Maximal projection was performed using the maximal projection function of ImageJ. For imaging of mitochondrial and ER morphology in S2 cells expressing RNAi-resistant Marf, cells expressing ER-GFP or mtGFP were excited using the 488-nm line of the laser of a confocal spinning-disk microscope (Andromeda iMIC system; TILL Photonics) with exposure times of 200 ms by using a U Plan S Apochromat 60×, 1.35 NA objective (Olympus).

For tetramethyl methyl ester imaging, 10^6 S2R+ cells loaded with 20 nM tetramethyl methyl ester dissolved in HBSS for 30 min at 25°C were placed on the stage of an inverted microscope (IMT-2; Olympus) equipped with a Cell^R imaging system (Olympus). Cells were excited using a 525/20-nm band pass excitation filter, and emitted light was acquired using a 570-nm long pass filter with exposure times of 200 ms by using a U Plan S Apochromat 60×, 1.35 NA objective. Images were deconvolved as described in the previous paragraph.

Larvae confocal images were acquired using a confocal microscope (C1; Nikon) equipped with a 40×, 1.0 NA differential interference contrast (DIC), 60×, 1.4 NA DIC Plan Apochromat, and 100×, 1.4 NA DIC objective (Nikon) using the EZC1 acquisition and analysis software (Nikon) or a confocal microscope (TCS SP5; Leica) using the LAS AF software (Leica), a 63×, 1.4 NA objective, and the 488-nm laser line. Images in figures except for Fig. 4 (A and B), Fig. 5 (B, F, and L), Fig. S2 H, and Fig. S3 B were equalized using the autoadjust function of PhotoPaint (Corel). For electron microscopy, *Drosophila* brains and larvae were fixed in 4% paraformaldehyde and 2% glutaraldehyde and embedded in Epon, and EM images were acquired from thin sections using a transmission electron microscope (Tecnai 12; FEI).

FLIP

FLIP experiments were performed as previously described (Orso et al., 2009) with minor modifications. Experimental larvae expressing UAS-GFP-KDEL were dissected in Ca^2+-free HL3 medium (70 mM NaCl, 5 mM KCl, 20 mM MgCl_2, 10 mM NaHCO_3, 5 mM trehalose, 115 mM sucrose, and 5 mM Hepes, pH 7.2) containing 7 mM glutamate and analyzed using a confocal microscope (C1) with a 1.0 NA, 60× water immersion objective. Two different regions of infection (ROIs) for each genotype distributed along muscle 6 or 7 were selected and bleached by 20 iterations, at 100% laser power, followed by three scanning images every 15 s. The area of ROI in Marf^RNAi muscle was ~70% of the ROI area in control muscle to reflect the smaller size of Marf^RNAi larvae. To create fluorescence recovery curves, fluorescence intensities were transformed into a 0–100% scale.

Morphometric analysis

Morphometric analysis was performed with Imagetool 3.0 (University of Texas Health Science Center, San Antonio, TX). Images of cells expressing mtYFP or ER-YFP were thresholded by using the automatic threshold function. For morphometric analysis of mitochondria, the major axis length and the roundness index of each identified object were calculated. Cells were scored with elongated mitochondria when >50% of the objects in the image (i.e., mitochondria) displayed a major axis longer than 3 μm and a roundness index below 0.3 (maximum value is 1). For morphometric analysis of ER, major axis length and the elongation index of each identified object were calculated. Cells were scored with reticular ER when the major axis was longer than 5 μm and the elongation index was >4 of >50% of the identified objects.

Immunoblotting

24 h after transfection, cells were harvested and disrupted in radioimmunoprecipitation assay buffer (150 mM NaCl, 1% Nonidet P-40/0, 0.25% deoxycholate, 1 mM EDTA, and 50 mM Tris, pH 7.4) in the presence of complete protease inhibitor mixture (Sigma-Aldrich). 20 brains from larvae or 100 whole larvae for each genotype were used for protein extraction. Samples were rinsed in radioimmunoprecipitation assay buffer with complete protease inhibitor mixture (Roche) and 1 mM PMSF (Sigma-Aldrich), homogenized in a 1-ml glass/Teflon potter (Wheaton), and then spun at 7,000 g for 10 min. Supernatants were collected and boiled for 5 min in Laemmli buffer (4% sodium dodecyl sulfate, 20% glycerol, 10% 2-mercaptoethanol, and blue bromophenol). Extracted proteins were separated by 4–12% SDS-PAGE (NuPAGE; Invitrogen), transferred onto polyvinylidene difluoride (Bio-Rad Laboratories) membranes, and probed using the following antibodies: anti-Actin (1:2,000; EMD Millipore), anti-Myc (1:1,000 [BD] or 1:1,000 [Roche]), anti-V5 (1:1,000; Invitrogen), anti-Marf (1:500), anti-BiP/Grp78 (1:1,000; BD), and anti-BiP (1:500).

In vivo *Drosophila* treatments

TUDCA (EMD Millipore) or PBA (EMD Millipore) were added to regular *Drosophila* food at a final concentration of 15 and 7.5 mM. To induce ER stress in vivo, dissected larvae were exposed to HL3 solution containing 500 μM DTT (Sigma-Aldrich) for 4 h. For experiments of ER stress, S2R+ cells cultured in Schneider's medium were treated for 24 h with 1 μM thapsigargin (Sigma-Aldrich) and 400 μM TUDCA or 15 mM PBA.

Climbing activity

For each genotype tested, 10 flies were collected and placed into an empty vial with a line drawn 2 cm from the bottom of the tube. After a 1-h recovery period from anesthesia (saturating CO_2), flies were gently tapped to the bottom of the tube, and the number of flies that after 20 s successfully climbed above the 2-cm mark was recorded. 15 separate and consecutive trials were performed, and the results were averaged. At least 240 flies were tested for each genotype in each independent experiment.

Statistics

Data are presented as means ± SEM of n independent experiments. Statistical significance was determined using Student's t tests with α set at 0.05.

Online supplemental material

Fig. S1 provides insight into the efficacy, specificity, and morphological effects of Marf ablation in S2 cells. Fig. S2 shows that a different Marf[RNAi] line causes the same mitochondrial and ER changes in vivo as the main line used for this study. Fig. S3 provides evidence for ER and SR alterations in Marf-depleted brains and muscles. Online supplemental material is available at http://www.jcb.org/cgi/content/full/jcb.201306121/DC1.

References

Area-Gomez, E., M. Del Carmen Lara Castillo, M.D. Tambini, C. Guardia-Laguarta, A.J. de Groof, M. Madra, J. Ikenouchi, M. Umeda, T.D. Bird, S.L. Sturley, and E.A. Schon. 2012. Upregulated function of mitochondria-associated ER membranes in Alzheimer disease. *EMBO J.* 31:4106–4123. http://dx.doi.org/10.1038/emboj.2012.202

Brand, A.H., and N. Perrimon. 1993. Targeted gene expression as a means of altering cell fates and generating dominant phenotypes. *Development.* 118:401–415.

Cartoni, R., E. Arnaud, J.J. Médard, O. Poirot, D.S. Courvoisier, R. Chrast, and J.C. Martinou. 2010. Expression of mitofusin 2(R94Q) in a transgenic mouse leads to Charcot-Marie-Tooth neuropathy type 2A. *Brain.* 133:1460–1469. http://dx.doi.org/10.1093/brain/awq082

Casas-Tinto, S., Y. Zhang, J. Sanchez-Garcia, M. Gomez-Velazquez, D.E. Rincon-Limas, and P. Fernandez-Funez. 2011. The ER stress factor XBP1s prevents amyloid-beta neurotoxicity. *Hum. Mol. Genet.* 20:2144–2160. http://dx.doi.org/10.1093/hmg/ddr100

Cerqua, C., V. Anesti, A. Pyakurel, D. Liu, D. Naon, G. Wiche, R. Baffa, K.S. Dimmer, and L. Scorrano. 2010. Trichoplein/mitostatin regulates endoplasmic reticulum-mitochondria juxtaposition. *EMBO Rep.* 11:854–860. http://dx.doi.org/10.1038/embor.2010.151

Chen, H., S.A. Detmer, A.J. Ewald, E.E. Griffin, S.E. Fraser, and D.C. Chan. 2003. Mitofusins Mfn1 and Mfn2 coordinately regulate mitochondrial fusion and are essential for embryonic development. *J. Cell Biol.* 160:189–200. http://dx.doi.org/10.1083/jcb.200211046

Chen, H., A. Chomyn, and D.C. Chan. 2005. Disruption of fusion results in mitochondrial heterogeneity and dysfunction. *J. Biol. Chem.* 280:26185–26192. http://dx.doi.org/10.1074/jbc.M503062200

Chen, Y., G. Csordás, C. Jowdy, T.G. Schneider, N. Csordás, W. Wang, Y. Liu, M. Kohlhaas, M. Meiser, S. Bergem, et al. 2012. Mitofusin 2-containing mitochondrial-reticular microdomains direct rapid cardiomyocyte bioenergetic responses via interorganelle Ca(2+) crosstalk. *Circ. Res.* 111:863–875. http://dx.doi.org/10.1161/CIRCRESAHA.112.266585

Cipolat, S., O. Martins de Brito, B. Dal Zilio, and L. Scorrano. 2004. OPA1 requires mitofusin 1 to promote mitochondrial fusion. *Proc. Natl. Acad. Sci. USA.* 101:15927–15932. http://dx.doi.org/10.1073/pnas.0407043101

de Brito, O.M., and L. Scorrano. 2008. Mitofusin 2 tethers endoplasmic reticulum to mitochondria. *Nature.* 456:605–610. http://dx.doi.org/10.1038/nature07534

de Brito, O.M., and L. Scorrano. 2010. An intimate liaison: spatial organization of the endoplasmic reticulum-mitochondria relationship. *EMBO J.* 29:2715–2723. http://dx.doi.org/10.1038/emboj.2010.177

De Stefani, D., A. Raffaello, E. Teardo, I. Szabò, and R. Rizzuto. 2011. A forty-kilodalton protein of the inner membrane is the mitochondrial calcium uniporter. *Nature.* 476:336–340. http://dx.doi.org/10.1038/nature10230

Deng, H., M.W. Dodson, H. Huang, and M. Guo. 2008. The Parkinson's disease genes pink1 and parkin promote mitochondrial fission and/or inhibit fusion in *Drosophila. Proc. Natl. Acad. Sci. USA.* 105:14503–14508. http://dx.doi.org/10.1073/pnas.0803998105

Detmer, S.A., and D.C. Chan. 2007. Complementation between mouse Mfn1 and Mfn2 protects mitochondrial fusion defects caused by CMT2A disease mutations. *J. Cell Biol.* 176:405–414. http://dx.doi.org/10.1083/jcb.200611080

Detmer, S.A., C. Vande Velde, D.W. Cleveland, and D.C. Chan. 2008. Hindlimb gait defects due to motor axon loss and reduced distal muscles in a transgenic mouse model of Charcot-Marie-Tooth type 2A. *Hum. Mol. Genet.* 17:367–375. http://dx.doi.org/10.1093/hmg/ddm314

Dorn, G.W., II, C.F. Clark, W.H. Eschenbacher, M.Y. Kang, J.T. Engelhard, S.J. Warner, S.J. Matkovich, and C.C. Jowdy. 2011. MARF and Opa1 control mitochondrial and cardiac function in *Drosophila. Circ. Res.* 108:12–17. http://dx.doi.org/10.1161/CIRCRESAHA.110.236745

Friedman, J.R., L.L. Lackner, M. West, J.R. DiBenedetto, J. Nunnari, and G.K. Voeltz. 2011. ER tubules mark sites of mitochondrial division. *Science.* 334:358–362. http://dx.doi.org/10.1126/science.1207385

Hales, K.G., and M.T. Fuller. 1997. Developmentally regulated mitochondrial fusion mediated by a conserved, novel, predicted GTPase. *Cell.* 90:121–129. http://dx.doi.org/10.1016/S0092-8674(00)80319-0

Hamasaki, M., N. Furuta, A. Matsuda, A. Nezu, A. Yamamoto, N. Fujita, H. Oomori, T. Noda, T. Haraguchi, Y. Hiraoka, et al. 2013. Autophagosomes form at ER-mitochondria contact sites. *Nature.* 495:389–393. http://dx.doi.org/10.1038/nature11910

Hwa, J.J., M.A. Hiller, M.T. Fuller, and A. Santel. 2002. Differential expression of the *Drosophila* mitofusin genes *fuzzy onions (fzo)* and *dmfn. Mech. Dev.* 116:213–216. http://dx.doi.org/10.1016/S0925-4773(02)00141-7

Inden, M., Y. Kitamura, H. Takeuchi, T. Yanagida, K. Takata, Y. Kobayashi, T. Taniguchi, K. Yoshimoto, M. Kaneko, Y. Okuma, et al. 2007. Neurodegeneration of mouse nigrostriatal dopaminergic system induced by repeated oral administration of rotenone is prevented by 4-phenyl-butyrate, a chemical chaperone. *J. Neurochem.* 101:1491–1504. http://dx.doi.org/10.1111/j.1471-4159.2006.04440.x

Irwin, W.A., N. Bergamin, P. Sabatelli, C. Reggiani, A. Megighian, L. Merlini, P. Braghetta, M. Columbaro, D. Volpin, G.M. Bressan, et al. 2003. Mitochondrial dysfunction and apoptosis in myopathic mice with collagen VI deficiency. *Nat. Genet.* 35:367–371. http://dx.doi.org/10.1038/ng1270

Ishihara, N., Y. Eura, and K. Mihara. 2004. Mitofusin 1 and 2 play distinct roles in mitochondrial fusion reactions via GTPase activity. *J. Cell Sci.* 117:6535–6546. http://dx.doi.org/10.1242/jcs.01565

Ishikawa, F., T. Akimoto, H. Yamamoto, Y. Araki, T. Yoshie, K. Mori, H. Hayashi, K. Nose, and M. Shibanuma. 2009. Gene expression profiling identifies a role for CHOP during inhibition of the mitochondrial respiratory chain. *J. Biochem.* 146:123–132. http://dx.doi.org/10.1093/jb/mvp052

Kasahara, A., S. Cipolat, Y. Chen, G.W. Dorn II, and L. Scorrano. 2013. Mitochondrial fusion directs cardiomyocyte differentiation via calcineurin and Notch signaling. *Science.* 342:734–737. http://dx.doi.org/10.1126/science.1241359

Kornmann, B., E. Currie, S.R. Collins, M. Schuldiner, J. Nunnari, J.S. Weissman, and P. Walter. 2009. An ER-mitochondria tethering complex revealed by a synthetic biology screen. *Science.* 325:477–481. http://dx.doi.org/10.1126/science.1175088

Ngoh, G.A., K.N. Papanicolaou, and K. Walsh. 2012. Loss of mitofusin 2 promotes endoplasmic reticulum stress. *J. Biol. Chem.* 287:20321–20332. http://dx.doi.org/10.1074/jbc.M112.359174

Olichon, A., L.J. Emorine, E. Descoins, L. Pelloquin, L. Brichese, N. Gas, E. Guillou, C. Delettre, A. Valette, C.P. Hamel, et al. 2002. The human dynamin-related protein OPA1 is anchored to the mitochondrial inner membrane facing the inter-membrane space. *FEBS Lett.* 523:171–176. http://dx.doi.org/10.1016/S0014-5793(02)02985-X

Orso, G., D. Pendin, S. Liu, J. Tosetto, T.J. Moss, J.E. Faust, M. Micaroni, A. Egorova, A. Martinuzzi, J.A. McNew, and A. Daga. 2009. Homotypic fusion of ER membranes requires the dynamin-like GTPase atlastin. *Nature.* 460:978–983. http://dx.doi.org/10.1038/nature08280

Osterwalder, T., K.S. Yoon, B.H. White, and H. Keshishian. 2001. A conditional tissue-specific transgene expression system using inducible GAL4. *Proc. Natl. Acad. Sci. USA.* 98:12596–12601. http://dx.doi.org/10.1073/pnas.221303298

Ozcan, U., E. Yilmaz, L. Ozcan, M. Furuhashi, E. Vaillancourt, R.O. Smith, C.Z. Görgün, and G.S. Hotamisligil. 2006. Chemical chaperones reduce ER stress and restore glucose homeostasis in a mouse model of type 2 diabetes. *Science.* 313:1137–1140. http://dx.doi.org/10.1126/science.1128294

Papanicolaou, K.N., R.J. Khairallah, G.A. Ngoh, A. Chikando, I. Luptak, K.M. O'Shea, D.D. Riley, J.J. Lugus, W.S. Colucci, W.J. Lederer, et al. 2011. Mitofusin-2 maintains mitochondrial structure and contributes

to stress-induced permeability transition in cardiac myocytes. *Mol. Cell. Biol.* 31:1309–1328. http://dx.doi.org/10.1128/MCB.00911-10

Ranganayakulu, G., R.A. Schulz, and E.N. Olson. 1996. Wingless signaling induces nautilus expression in the ventral mesoderm of the *Drosophila* embryo. *Dev. Biol.* 176:143–148. http://dx.doi.org/10.1006/dbio.1996.9987

Ryoo, H.D., P.M. Domingos, M.J. Kang, and H. Steller. 2007. Unfolded protein response in a *Drosophila* model for retinal degeneration. *EMBO J.* 26:242–252. http://dx.doi.org/10.1038/sj.emboj.7601477

Ryoo, H.D., J. Li, and M.J. Kang. 2013. *Drosophila* XBP1 expression reporter marks cells under endoplasmic reticulum stress and with high protein secretory load. *PLoS ONE*. 8:e75774. http://dx.doi.org/10.1371/journal.pone.0075774

Santel, A., and M.T. Fuller. 2001. Control of mitochondrial morphology by a human mitofusin. *J. Cell Sci.* 114:867–874.

Santel, A., S. Frank, B. Gaume, M. Herrler, R.J. Youle, and M.T. Fuller. 2003. Mitofusin-1 protein is a generally expressed mediator of mitochondrial fusion in mammalian cells. *J. Cell Sci.* 116:2763–2774. http://dx.doi.org/10.1242/jcs.00479

Schneeberger, M., M.O. Dietrich, D. Sebastián, M. Imbernón, C. Castaño, A. Garcia, Y. Esteban, A. Gonzalez-Franquesa, I.C. Rodríguez, A. Bortolozzi, et al. 2013. Mitofusin 2 in POMC neurons connects ER stress with leptin resistance and energy imbalance. *Cell*. 155:172–187. http://dx.doi.org/10.1016/j.cell.2013.09.003

Sebastián, D., M.I. Hernández-Alvarez, J. Segalés, E. Sorianello, J.P. Muñoz, D. Sala, A. Waget, M. Liesa, J.C. Paz, P. Gopalacharyulu, et al. 2012. Mitofusin 2 (Mfn2) links mitochondrial and endoplasmic reticulum function with insulin signaling and is essential for normal glucose homeostasis. *Proc. Natl. Acad. Sci. USA*. 109:5523–5528. http://dx.doi.org/10.1073/pnas.1108220109

Snapp, E.L., T. Iida, D. Frescas, J. Lippincott-Schwartz, and M.A. Lilly. 2004. The fusome mediates intercellular endoplasmic reticulum connectivity in *Drosophila* ovarian cysts. *Mol. Biol. Cell*. 15:4512–4521. http://dx.doi.org/10.1091/mbc.E04-06-0475

Solá, S., R.E. Castro, P.A. Laires, C.J. Steer, and C.M. Rodrigues. 2003. Tauroursodeoxycholic acid prevents amyloid-beta peptide-induced neuronal death via a phosphatidylinositol 3-kinase-dependent signaling pathway. *Mol. Med.* 9:226–234.

Tondera, D., S. Grandemange, A. Jourdain, M. Karbowski, Y. Mattenberger, S. Herzig, S. Da Cruz, P. Clerc, I. Raschke, C. Merkwirth, et al. 2009. SLP-2 is required for stress-induced mitochondrial hyperfusion. *EMBO J.* 28:1589–1600. http://dx.doi.org/10.1038/emboj.2009.89

Ziviani, E., R.N. Tao, and A.J. Whitworth. 2010. *Drosophila* parkin requires PINK1 for mitochondrial translocation and ubiquitinates mitofusin. *Proc. Natl. Acad. Sci. USA*. 107:5018–5023. http://dx.doi.org/10.1073/pnas.0913485107

Züchner, S., I.V. Mersiyanova, M. Muglia, N. Bissar-Tadmouri, J. Rochelle, E.L. Dadali, M. Zappia, E. Nelis, A. Patitucci, J. Senderek, et al. 2004. Mutations in the mitochondrial GTPase mitofusin 2 cause Charcot-Marie-Tooth neuropathy type 2A. *Nat. Genet.* 36:449–451. http://dx.doi.org/10.1038/ng1341